Kinetic, Products and Shrinkage for the Pyrolysis of Flax Fibers

Asma Dhahak, Laurent Cezard, Stéphanie Baumberger, Jorge Peixinho

Graphical Abstract

Kinetic, Products and Shrinkage for the Pyrolysis of Flax Fibers

Asma Dhahak, Laurent Cézard, Stéphanie Baumberger, Jorge Peixinho

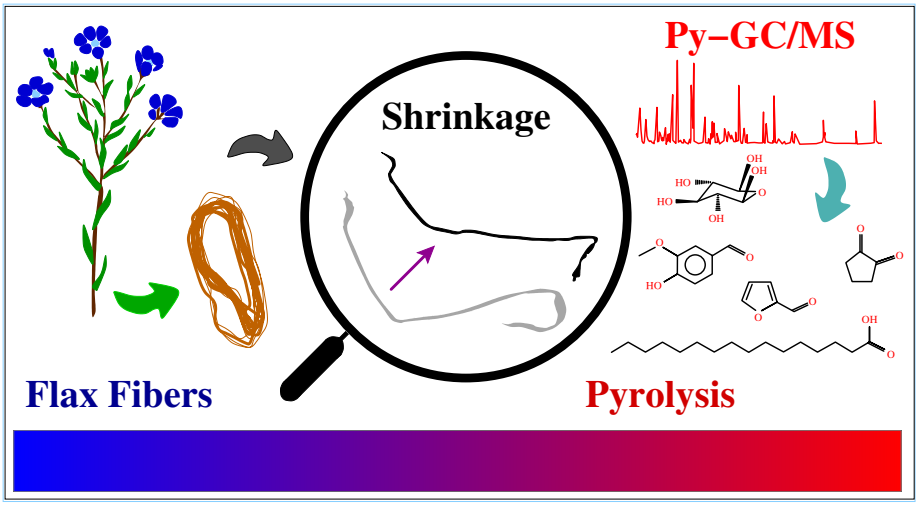

Highlights

Kinetic, Products and Shrinkage for the Pyrolysis of Flax Fibers

Asma Dhahak, Laurent Cézard, Stéphanie Baumberger, Jorge Peixinho

- Insights into flax fibers pyrolysis at different heating rates are reported.
- The thermal behavior, the morphological evolution and the shrinkage are presented.
- The product characterisation of flax fibers has been obtained by Py-GC/MS.
- The shrinkage is related to the production of furans and ketones.

Kinetic, Products and Shrinkage for the Pyrolysis of Flax Fibers

Asma Dhahak[a], Laurent Cézard[b], Stéphanie Baumberger[b], Jorge Peixinho[a,*]

[a] *Laboratoire PIMM, CNRS, Arts et Métiers Institute of Technology, Cnam, HESAM Université, Paris, 75013, France*
[b] *Université Paris-Saclay, INRAE, AgroParisTech, Institut Jean-Pierre Bourgin (IJPB), Versailles, 78000, France*

Abstract

Biomass pyrolysis is a thermochemical process used for renewable products and energies. However, there are still issues that need to be addressed for process modeling and optimization. This study focuses on the relationship between heating rate, shrinkage, and products from flax fibers using thermogravimetric analysis (TGA), microscopic observation, and pyrolysis-gas chromatography/mass spectrometry (Py-GC/MS). TGA confirms sequential evaporation of water then decomposition of hemicellulose, cellulose, and lignin. Observations from the micro-reactor show that flax fibers undergo shrinkage within the temperature range of 335 to 370 °C, depending on the heating rate. Pyrolysis products were analyzed using Py-GC/MS at four different final temperatures from 350 to 500 °C, revealing the presence of anhydrosugars, furans, ketones, phenols, esters, alcohols, aldehydes, and acids. The results indicate a correlation between temperature and the increase in furans and ketones. The analysis suggests that furans and ketones are associated with shrinkage.

Keywords: Pyrolysis, flax fibers, shrinkage, Py-GC/MS

1. Introduction

Lignocellulosic biomass, derived from sources such as wood, agricultural waste, and energy crops, is a renewable source of energy, materials and chemicals due to its abundance and cost-effectiveness [1]. Pyrolysis, which is the thermal degradation of the biomass at high temperatures in non-oxidizing conditions [2], produces valuable chemical compounds, including bio-oil, bio-char, and gas [3]. Numerous studies have investigated the pyrolysis of various types of lignocellulosic biomass and the effects of different factors on product yields and qualities [2, 4, 5]. Non-woody biomass is a promising feedstock for biofuel production due to its low lignin con-

*Corresponding author.
Email address: jorge.peixinho@cnrs.fr (J. Peixinho)

tent. Although lignin provides structural strength and rigidity to plant cell walls, it also hinders the conversion of cellulose and hemicellulose into fermentable sugars. Therefore, in biofuel processes, it is often necessary to remove lignin, which requires energy and chemicals [6, 7].

Flax natural fibers are commonly used in various applications, such as textiles, high-quality paper production, construction, and automotive industry [8]. Actually, flax fibers are one of the strongest natural fibers, making them a potential replacement for glass fiber in composite materials [9]. The majority of these fibers are sourced from Europe, which accounted for 97 % of the global flax output from 2018 to 2019, while Asia and Africa contributed 2 % and 1 %, respectively [10]. Flax fiber is composed of varying amounts of cellulose, hemicellulose, and lignin, along with minor quantities of other components such as pectin and wax. Cellulose is the most abundant component, accounting for about 65 to 80 %, followed by hemicellulose at 14 to 21 %, and lignin at 1 to 3 % [11]. Flax fiber contains hemicellulose-specific carbohydrates such as mannose, xylose, and galactose, while pectin contains arabinose and galactose [12]. The main sugar unit of cellulose, glucose, is also present as hemicellulosic constituent. During pyrolysis, volatile compounds are primarily released by cellulose and hemicellulose, while char production is favored by the presence of lignin [13]. The pyrolysis of cellulose leads to the formation of anhydrosugars, furan derivatives, water, and light oxygenated species [14]. Levoglucosan is the main anhydrosugar component that is predominately induced at low temperatures and its production declines [15] when the temperature exceeds 530 °C. Two other major products obtained during cellulose pyrolysis are hydroxyacetaldehyde and 5-hydroxymethyl-furfural [16]. Concerning the degradation of hemicellulose, the main volatile products released from xylan-based hemicellulose are carbon monoxide (CO), carbon dioxide (CO_2), methane (CH_4), methanol, furfural and acetic acid [17, 18]. Regarding the pyrolysis of lignin, the most stable thermal compound, the degradation takes place at temperatures ranging from 300 to 550 °C, generating a variety of aromatic compounds (phenolics and hydrocarbons) [17, 19, 3]. Del Rio et al. [20, 21] characterized the products released during the pyrolysis of lignin isolated from flax fiber using Pyrolysis-Gas chromatography/Mass spectrometry (Py-GC/MS). The results showed the predominance of guaiacol and its derivatives, vanillin and syringol. These compounds have high heating value and can be used as additives for bio-oil upgrading or stabilization. Additionally, the pyrolysis of flax fiber produces CO_2, CO, formaldehyde, acetic and formic acids and water [22]. Reed et al. [13] also investigated the slow pyrolysis of many natural fibers, including flax fibers, using a fixed bed reactor. They found that flax fiber degradation produced mainly CO_2 with 76 %, followed by CO with 13 % and CH_4 with 2.3 %.

Biomass pyrolysis has been extensively studied using various reactor configurations, including micro-reactors, such as micro-tubular reactors, spray-bed reactors and

fixed-bed mini-reactors [23, 24]. However, the use of hot pyrolysis micro-reactors with an optical microscope has rarely been used, to our knowledge, on biomass pyrolysis [12, 25, 26, 27]. Hot stage microscopy combines thermal analysis and microscopy to characterize the solid state of materials in terms of temperature and time. It enables monitoring during the thermal reaction using an optical microscope, a camera, and a control software [3]. This technique can complement thermal techniques such as thermogravimetry analysis (TGA) and differential scanning calorimetry, allowing observation of phenomena such as surface changes, phase transitions and recrystallization.

Recent modelling studies now consider the coupling of gas flow through a porous media, heat transfer and reaction kinetic models. These models are often in the form of first-order single-step reactions [28, 29, 30]. Recent multicomponent pyrolysis models [31] accurately replicate thermogravimetric data of lignocellulosic biomass. However, during pyrolysis, the emergence of shrinking volumes, changing solid geometry and varying pore structure during pyrolysis results in a reduction of the active surface area. This limits the hypotheses of constant apparent reaction rates. Data on the shrinking ratio should help to adapt and optimize the prediction of pyrolysis mechanism and kinetics of flax fiber and its components.

This paper investigated various factors, such as heating rate and temperature. The morphological evolution of the fiber during pyrolysis at different heating rates was examined using an optical microscope micro-reactor. Additionally, the structural and compositional analysis of volatile compounds during flax fiber pyrolysis at different temperatures was conducted using Py-GC/MS. The aim of the analysis was to identify the predominant reactions and compounds responsible for the shrinkage of fibre length and mass loss as a function of temperature.

2. Materials and Methods

2.1. Material

The flax fibers used in the study were obtained from Flax Technic, Depestele (Normandie, France). Elemental analysis revealed that flax fibers contained 41.8 % carbon, 7.1 % hydrogen and 51.1 % of oxygen. The fibers were utilized as received and stored at room temperature before the experiments.

2.2. Thermogravimetric Analysis (TGA)

Thermogravimetric analysis (TGA) was performed using a TA instrument Q500. The final set temperature was 600 °C, and the sample was subjected to different heating rates: 5, 10, 20 and 50 °C/min. The nitrogen flow rate was maintained at 90 mL/min. A bundle of fibers, with an initial mass ranging between 5 to 8 mg, was introduced into a platinum crucible of 100 μL.

2.3. Hot Stage Pyrolysis Micro-Reactor

The experimental setup involves extracting one fiber from bundles and placing it in a hot stage micro-reactor (Linkam cell THMS600) between two thin glass slides, mounted on a Nikon optical microscope. Liquid nitrogen was used as inert gas. The sample was heated

to 500 °C at five different heating rates from 10 to 150 °C/min. The heating plate, about 22 mm in diameter, had an inserted 2 mm quartz disk upon which the fiber was placed. Transmitted light passed through the sample and was collected from above with a 10x magnification optic. During heating, the sample was observed using a color video camera with a resolution of 1200×1600 pixels, and images were obtained as a function of temperature and time.

2.4. Pyrolysis-Gas Chromatography/Mass Spectrometry (Py-GC/MS)

Analyses were carried out using a CDS model 5250 306 pyroprobe autosampler 307 interfaced to an Agilent 6890/5973 GC/MS. Several milligrams of flax fibers were ground using a coffee bean micronizer. Approximately 1.6±0.2 mg of the ground flax fiber was then introduced in a quartz tube of the pyrolyzer. Each sample was initially heated at a constant temperature for 15 seconds with helium as a carrier gas at a flow rate of 1 mL/min. Four final temperatures were tested: 350, 400, 450, and 500 °C. The volatile pyrolysis products were separated using a split ratio of 10:1 and a GC capillary column HP-5 MS (5 % phenyl methyl siloxane, 30 m, 250 μm i.d., and 0.25 μm film thickness, Agilent Technologies) with helium as the carrier gas (flow rate of 1 mL/min). The pyrolysis and GC/MS interfaces were kept at 290 °C and the GC was temperature-programmed from 30 °C (for 1 min) to 130 °C at 6 °C/min, then from 130 to 250 °C at 12 °C/min and finally from 250 °C to 300 °C at 30 °C/min (3 min at 300 °C). The MS was operated in the electron impact mode (70 eV) for m/z 40 to 450.

3. Results and Discussion

3.1. Thermogravimetric Analysis

The TGA and DTG curves of the pyrolysis of flax fiber bundles were presented in Figure 1. Typically, a short number of fibers were cut and arranged to fit into the sample pan. The pyrolysis process showed four distinct stages of weight loss, which was consistent with previous studies [32, 22]. The first stage, which occurred at around 100 °C, corresponded to the evaporation of moisture from the fibers, resulting in 4.2 % mass loss. The second stage of the process was attributed to the degradation of hemicellulose, resulting in the release of volatile compounds. The DTG curve showed a significant weight loss between 250 and 350 °C, showing a mass loss of 4 % at 50 °C/min and 7.1 % at 5 °C/min. This stage was characterized by the production of volatile species, mainly CO and CO_2 from the decomposition of hemicellulose. The third stage, which ranged from 300 to 420 °C, was associated with cellulose degradation. At a heating rate of 50 °C/min, the mass lost approximately 60 % of its mass at 406 °C. The decomposition of cellulose involved several reactions, including depolymerization, dehydration, decarboxylation, and aromatization. The fourth stage, occurring between 250 and 600 °C, was the longest decomposition stage. This was attributed to the slow degradation of lignin due to its heterogeneity and its cross-linked structure involving C-C and ether linkages [33].

Figure 1 illustrated that when the heating rate increases, the DTG curves remarkably moved toward higher values, resulting in an increase in the maximum pyrolysis rate. This was in line with previous research [34]. The DTG maximum curves at heating rates of 5, 10, 20 and 50 °C/min, were 355, 368, 385, and 406 °C, respectively. The TGA curves indicated that the residual at 600 °C is constant between 14 to 16 %, in good agreement with previous studies [35].

3.2. Pyrolysis using the Hot Stage Microscopy

During the pyrolysis process in the hot stage microscope, the sample experiences gradual and continuous heating under controlled atmosphere. The changes in the physical properties of the sample were observed and recorded by a camera attached to the microscope over time and temperature. Figure 2 displayed images before and after pyrolysis, at 10 °C/min and 150 °C/min. Such high heating rate are preferred for bio-oil production [36]. The morphological evolution of flax fiber, particularly in terms of length and diameter, was significant. Clearly, as the temperature increases above 100 °C, hydrogen bonds networks and cellulose backbone (C-O stretching) are destabilized [37]. At high temperature above 300 °C, the fiber changed color to black. For example, at a heating rate of 10 °C/min, the color darkened between 320 and 370 °C, whereas at 150 °C/min, it darkened between 380 and 420 °C. This darkening was attributed to the carbonization of the flax fiber. Furthermore, when the fiber reached complete darkness, it exhibited movement and shrinkage.

To clearly demonstrate the morphological evolution during pyrolysis, the shrinkage ratio, S, based on the total fiber length was calculated from the imaged following the equation:

$$S\,(\%) = \frac{L(t) - L_0}{L_0}, \tag{1}$$

where $L(t)$ was the instantaneous fiber length and L_0 was the initial length. Again the experimental time duration is directly proportional to the temperature. Figure 3 illustrated the thermal evolution of shrinkage under different heating rates. Each data point corresponded to a specific number of images analyzed by the ImageJ software [38]. The error bars represented the dispersion over at least three repetitions of the experiments. Below 200 °C, there was no significant change in fiber length. However, at higher temperatures and slower heating rates, particularly at 10 and 20 °C/min, a small peak was observed before a notable increase in shrinkage. The peak temperature was observed between 335 and 370 °at a heating rate of 10 °/min and between 360 and 391 °at a heating rate of 20 °/min. This indicated a gradual degradation of the fiber components, which affected the shrinkage rate. Moreover, the shrinkage curves shifted towards higher temperatures as the heating rate increased, exhibiting similar behavior for all heating rates. For example, the temperature at which the shrinkage rate began to increase (T_{start}) was around 375, 381 and 401 °C at 50, 100 and 150 °C/min, respectively. Beyond T_{start}, the shrinkage increased rapidly and then decelerated to reach

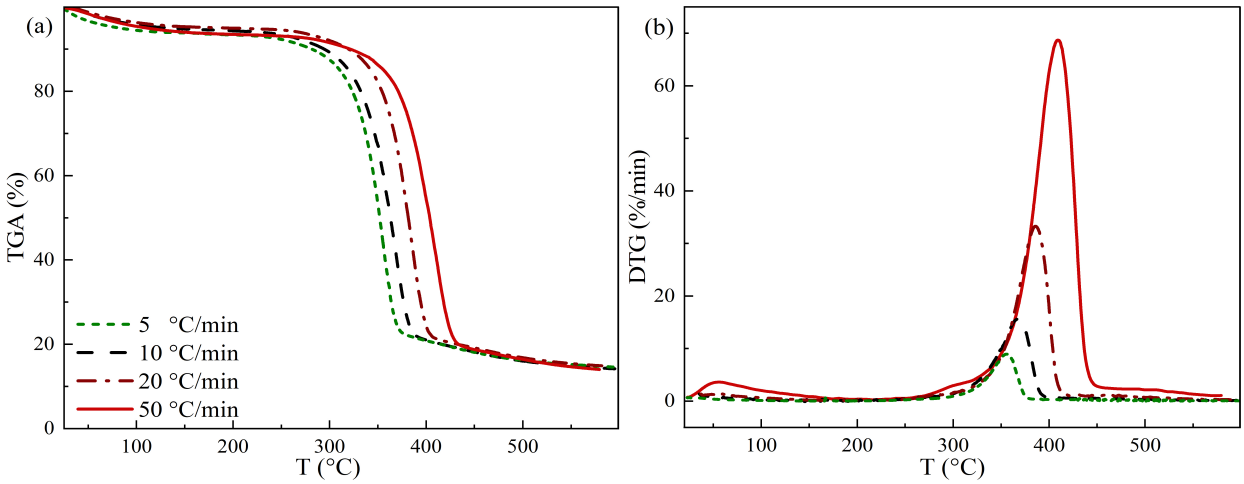

Figure 1: (a) Thermogravimetric analysis (TGA) and (b) Derivative Thermogravimetric analysis (DTG) of flax fibers at different heating rates

approximately 13 % at 500 °C. The inset in Figure 3 showed T_{start} as a function of heating rates β. It can be observed that T_{start} shifted to higher temperatures with increasing heating rates in a quadratic fashion.

3.3. Pyrolysis-Gas Chromatography/Mass Spectrometry (Py-GC/MS)

Chromatograms of flax fiber pyrolysis at different temperatures (350, 450 and 500 °C) are presented in Figure 4. The majority of peaks were identified using the Nist library and previous studies [39, 35, 40]. The main compounds identified were listed in Table 1, with 40 peaks identified. The Py-GC/MS analysis revealed a diverse range of chemical categories, including anhydrosugars, furans, esters, alcohols, acids, aldehydes, and phenols. Other families included nitrogen compounds, such as 2,2-diethyl-3-methyl-oxazolidine, alkanes and alkenes. The pyrolysis of cellulose resulted in the formation of anhydrosugars, while the degradation of hemicellulose produced acids, ketones, and esters. Furthermore, the primary categories of lignin degradation products were phenols and aldehydes [41]. The furan category, which was derived from the pyrolysis of cellulose and hemicellulose, produced abundant products, including furfural (peak 6), 2-furanmethanol (peak 7), and 5-hydroxymethylfurfural (peak 26). Ketones yielded 1,2-cyclopentanedione (peak 10), while alcohols produced 3-buten-1,2-diol (peak 19). Within the anhydrosugar family, 1,4:3,6-dianhydro–α–D-glucopyranose (peak 23) and levoglucosan (peak 35) were present. The category of phenol included catechol (peak 24), 4-vinylguaiacol (peak 30), syringol (peak 31), vanillin (peak 33), trans-Isoeugenol (peak 34) and coniferyl aldehyde (peak 38). The aldehyde category included

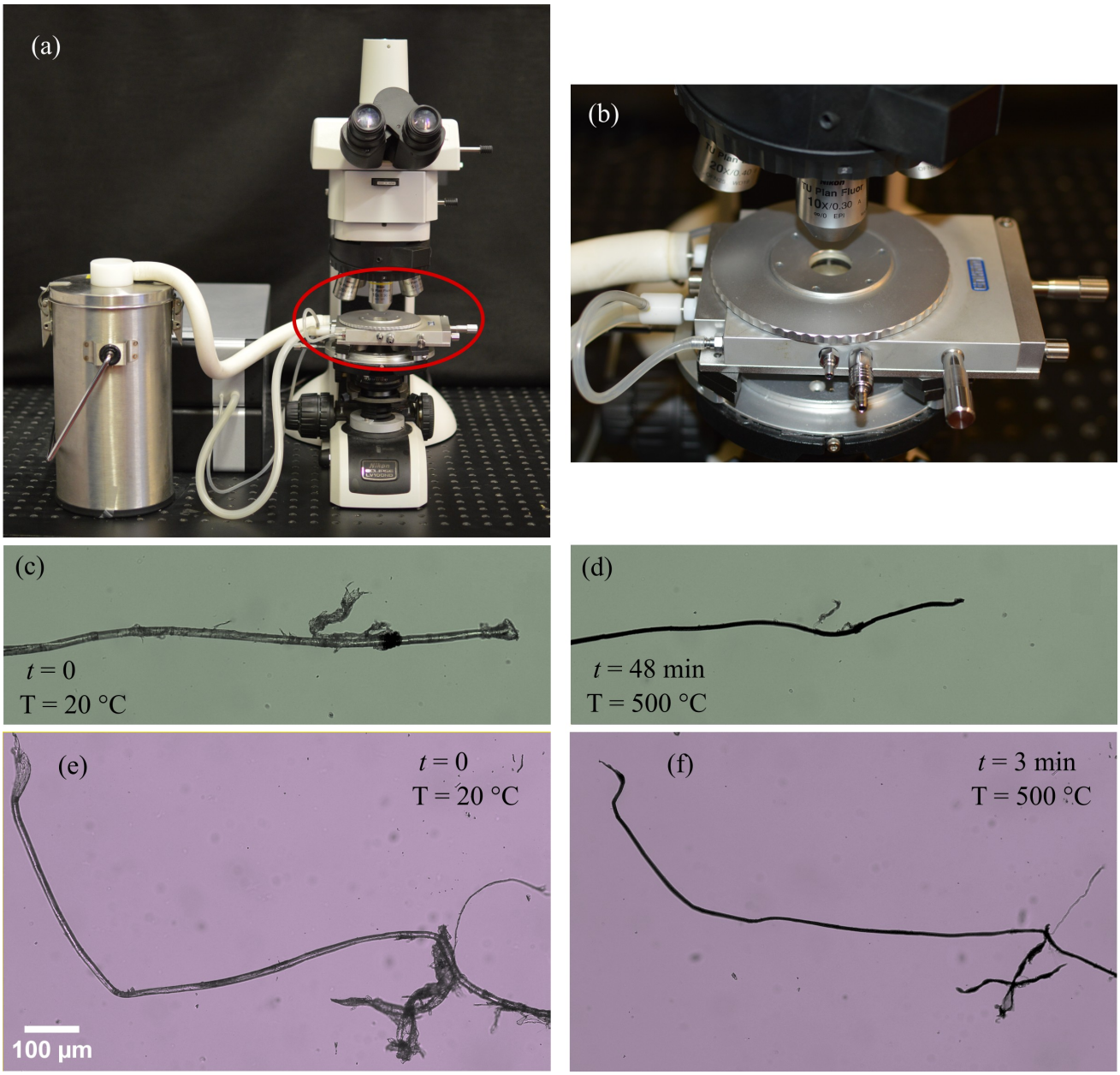

Figure 2: Photograph of the hot stage microscope with the nitrogen gas reservoir (a) and a zoom of the micro-reactor (b). Images of the flax fiber before and after pyrolysis at 10 °C/min (c-d) and 150 °C/min (e-f).

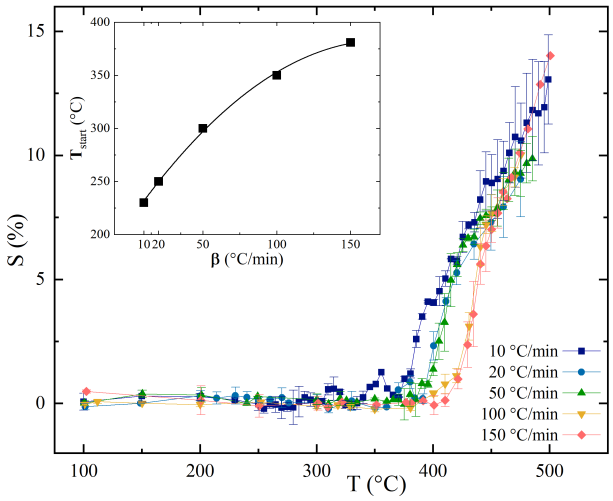

Figure 3: The evolution of fiber shrinkage as a function of temperature at different heating rates. The inset represented the onset of shrinkage as a function of the heating rate

2-butenal, 2-methyl (peak 1), while the acid family featured palmitic acid (peak 40).

Figure 5 presented the evolution of the relative abundance of chemical families. At low temperatures, the most abundant chemical families were esters, furans, ketones, aldehydes and anhydrosugars. As the temperature increased, the relative abundance of ketones and furans increased, while the proportion of aldehydes remained relatively stable from 350 to 500 °C. Alcohols became prevalent above 400 °C, and then their relative abundance remained stable thereafter. Among the ester category, diethyl terephthalate, was detected at low temperatures, indicating the degradation of hemicellulose [41]. The phenol family was present at low temperatures, but decreased from 400 to 450 and then slightly increased at 500 °C. Acids appeared at 450 °C, and their relative abundance decreased significantly at 500 °C.

The evolution of relative abundance in each category was illustrated in Figure 6. The anhydrosugar family results showed that at 350 °C, only levoglucosan (1,6-anhydro-β-d-glucopyranose) was identified, thereby confirming its status as the primary product of the depolymerization reaction during cellulose pyrolysis. This finding was in good agreement with previous researches [42, 43]. At 400 °C, no compounds from this category were detected, indicating that levoglucosan undergoes chemical reactions at this temperature range, including ring-opening to produce small molecular gases such as CO, CO_2, and acetaldehyde, which are undetectable by Py-GC/MS [44]. Levoglucosan can be transformed into other anhydro-monosaccharides through dehydration and isomerization reactions, such as dianhydro-β-d-glucopyranose, which appeared at 400 °C [45, 46]. The synthesis of 1,2:5,6-dianhydrogalactitol was suggested to result from the deoxygenation of anhydrosugars, such as levoglucosan [47]. This compound was detected at 400 °C. This suggested that levoglucosan served as an intermediary in the formation of other products during cellulose pyrolysis [48]. Furthermore, the degradation of levoglucosan led to the formation of 5-hydroxymethylfurfural (5-HMF), which can further yield furfural [48]. In addition, levoglucosan can also form through subsequent reactions of anhydrosugars, which was observed again at around 500 °C. Furan compounds, such as furanmethanol, furaldehyde, furfural, (5H)-furanone, and 5-HMF, were detected above 350 °C. The dom-

inant compound in this category was 2-Furanmethanol, representing 36 % of the total furans at 400 °C. Its proportion decreased from 450 to 500 °C. The percentage of furfural varied between 14 and 20 % at temperatures ranging from 400 to 500 °C. However, the proportion of 5-HMF increased until 10 % at 500 °C. Furfural and 5-HMF may be produced through dehydration, depolymerization, and rearrangement reactions of cellulose [49]. Various derivatives of the phenol family were formed at different temperatures as a result of lignin decomposition. When the temperature was lowered to 350 °C, guaiacol derivatives such as 4-vinylguaiacol and p-propylguaiacol appeared. These guaiacol compounds were produced through the depolymerization and dehydration reactions of lignin [50]. At 500 °C, catechol and its derivatives became the main phenol compounds, with the presence of 4-vinyl-guaiacol, vanillin, trans-Isoeugenol and syringol. This demonstrated that the formation of catechol was enhanced at high temperatures due to the demethylation reactions of the guaiacyl unit, explaining the decrease of relative peaks of guaiacol derivatives, specifically for p-propylguaiacol between 350 to 500 °C [50]. This was in agreement with other studies on different biomass [51]. These phenolic compounds can be categorized into four substructures: syringyl (S-type), p-hydroxyphenyl-type (H-type), guaiacol-type (G-type) and catechol-type (C-type). The dominant substructure identified was the G-type, which was consistent with previous studies [21]. At 500 °C, the S/G ratio, calculated from the area peak, was around 0.05 and H/G was 0.13. In the ketone category, the presence of p-octylacetophenone was observed at 350 °C, and its proportion decreased as temperature increased. Subsequently, at 400 °C, 1,2-cyclopentanedione became the dominant product in this chemical family, with its proportion also decreasing with rising temperature. The formation of 1,2-cyclopentanedione can occur through the cyclization subsequent to the opening of the pyran ring [52].

3.4. Analysis: Combination of Shrinkage, DTG and Py-GC/MS

The physical and chemical changes that occur during the process can be comprehensively understood through the combination of fiber shrinkage, DTG and Py-GC/MS characterization. Note that during shrinkage, flax fibers are deposited on a quartz glass, while in the Py-GC/MS, the grounded flax is introduced in a quartz tube. So, the main difference between the experiments is the sample volume and the pretreatment. Yet, previous studies have showed that only specific chemical treatments are capable to modify the reaction rates and products of flax pyrolysis [35]. Figure 7(a) presented the relationships between the mass loss of flax fiber and the shrinkage behavior at low heating rates (10 and 50 °C/min). It had been demonstrated that for both the start of shrinkage in a microreactor and the degradation of flax fiber in DTG occurred approximately at the same temperature range. As the flax fiber decomposition reached its peak, significant shrinkage ensued, leading to a reduction in its length. Based on TGA studies and component range degradation, the degradation of

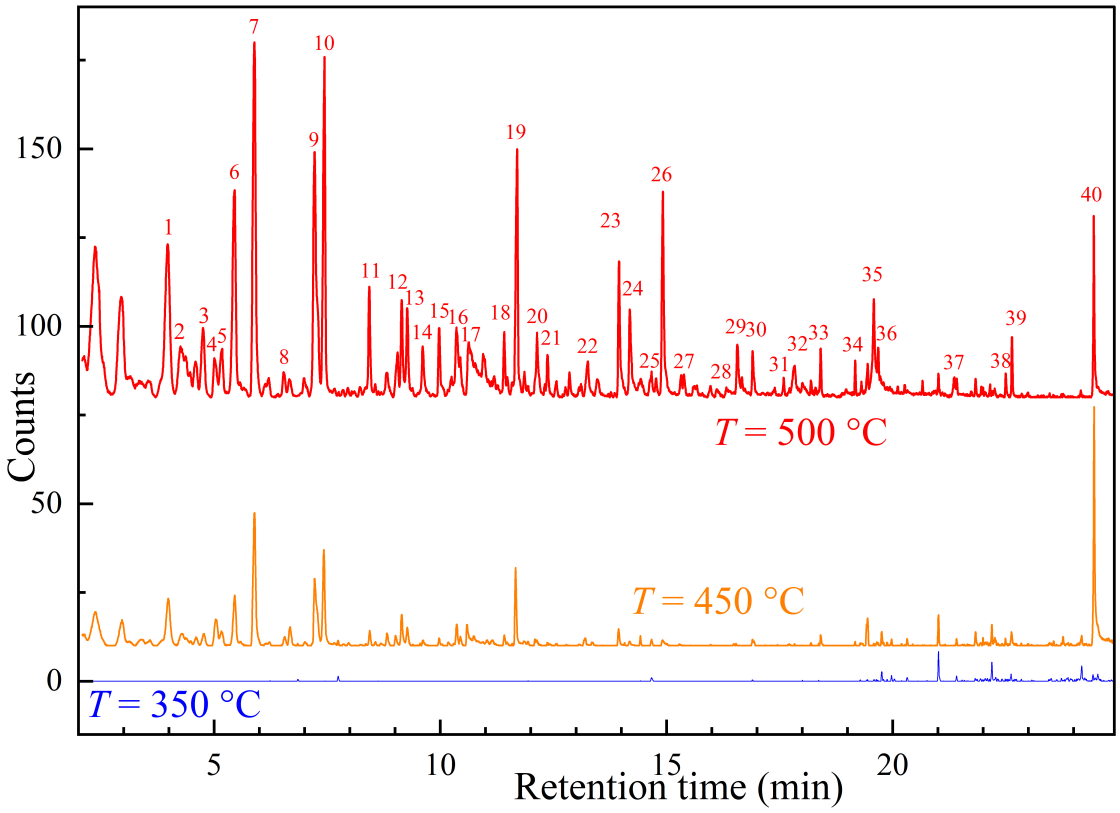

Figure 4: Chromatograms for flax fibers at 350, 450 and 500 °C, shifted vertically by 15 and 70, respectively

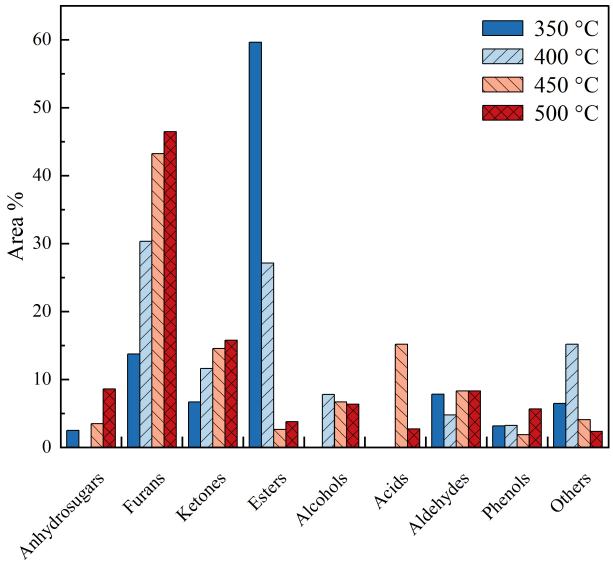

Figure 5: Evolution of the relative peak areas of different chemical categories at different temperatures

hemicellulose, cellulose, and lignin may be responsible for the fluctuations in shrinkage before the sharp increased in the curve. The pronounced shrinkage observed in the subsequent phase corresponded to the degradation of cellulose and lignin. At a higher heating rate of 150 °C/min, Figure 7(b) illustrated the combined effects of shrinkage and the thermal evolution of chemical categories. Initially, even before any shrinkage can be noticed, around 350 °C, the DTG curve increases and both furans and ketones relative concentrations already increase. However, the peak area of esters decreased as the temperature rose, indicating that esters did not contribute to the shrinkage behavior. Additionally, there was no significant variation in the relative peak area of phenols during this temperature range [53]. At 400 °C, several compounds exhibited high reactivity, including 1,4:3,6-dianhydro-d-glucopyranose and 1,2:5,6-dianhydrogalactitol from the anhydrosugar family, 5HMF and 2 (5H)-Furanone from the furan family, 2 H-pyran-2,6(3H)-dione, maltol, and 4-cyclopentene-1,3-dione from the ketone family, as well as 4-vinylguaiacol and vanillin from the phenols group. This suggested the involvement of these components in the shrinkage process. In this range, the predominant reactions may include the dehydration and isomerization of levoglucosan.

4. Conclusions

In this study, flax fibers were utilized as a model for biomass pyrolysis. TGA confirmed previous findings, showing sequential evaporation of water, followed by the degradation of hemicellulose, cellulose and lignin. The pyrolysis process was almost completed at 600 °C, resulting in a mass loss of around 75 %. Microscope observations were used to determine the shrinkage behavior and to observe the morphological evolution and degree of carbonization in the samples in real-time. The shrinkage curves moved towards higher temperatures and exhibited similar behaviors for all heating rates. Furthermore, Py-GC/MS analysis at various temperatures facilitated the identification and examination of the developement of several products. It was found that the main volatile categories formed were furans, ketones, anhydrosugars, esters, and phenols. The correlation between various phenomena in flax fibers was revealed through the combination of shrinkage, DTG,

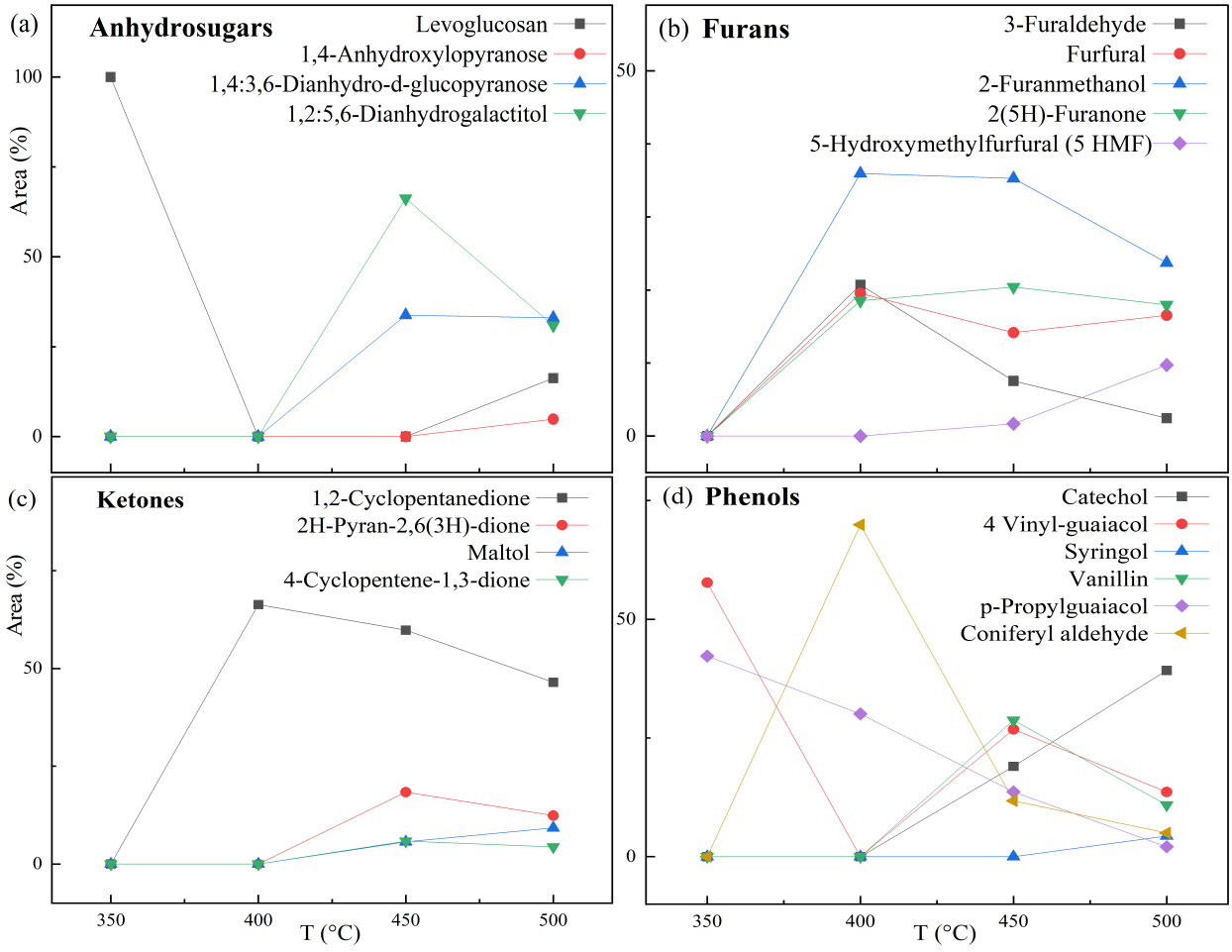

Figure 6: The thermal evolution of the main compounds in each category (a) Anhydrosugars, (b) Furans, (c) Ketones and (d) Phenols

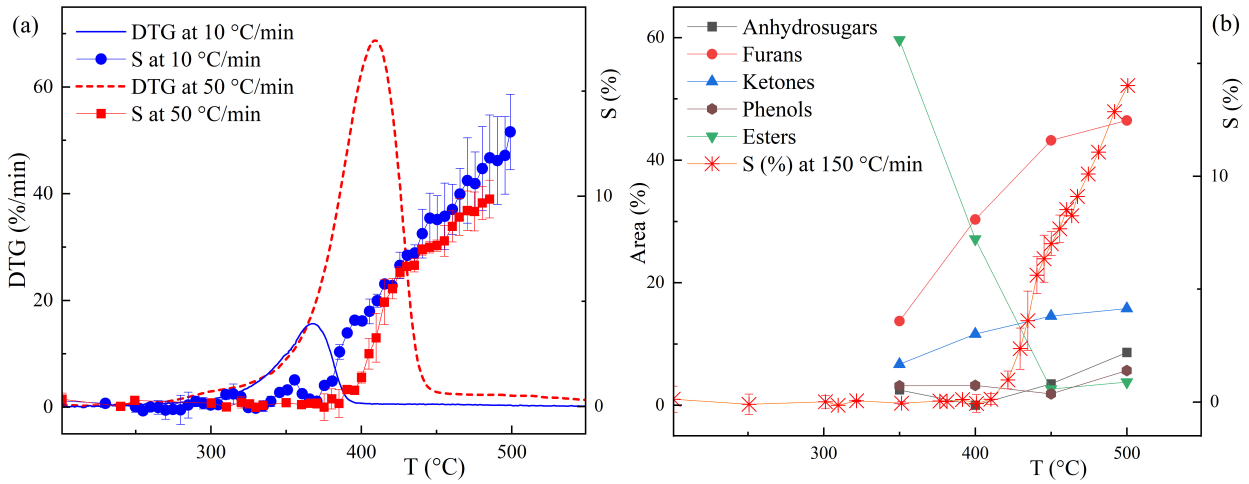

Figure 7: Superposition of (a) DTG and shrinkage at 10 and 50 °C/min versus temperature and (b) The evolution of relative area of the main categories by Py-GC/MS and shrinkage at 150 °C/min versus temperature.

and Py-GC/MS analysis. The maximum DTG was found to be closely correlated with the onset of rapid shrinkage. Additionally, a shift towards higher temperatures was observed for both the maximum DTG and the onset of shrinkage. These results, particularly in terms of shrinkage, provide valuable insights into possible heat and mass modeling, contributing to a comprehensive understanding of the pyrolysis of flax fibers.

CRediT authorship contribution statement

Asma Dhahak: Data curation, Analysis, Investigation, Writing. **Laurent Cézard:** Data curation, Analysis. **Stéphanie Baumberger:** Writing – review & editing. **Jorge Peixinho:** Methodology, Visualization, Resource, Supervision.

Declaration of Competing Interest

The authors declare that they have no known competing financial interests or personal relationships that could have appeared to influence the work reported in this paper.

5. Data availability

Data will be made available on request.

Acknowledgement

The authors acknowledge Prof. Julien Legros (COBRA) for conducting the elemental analysis of the flax fibers and Dr. Alain Guinault (PIMM) for his valuable contributions. The authors acknowledge the financial support of the Agence Nationale de la Recherche (ANR) through the PyroBioFuel project funded by the European Union's

Horizon 2020 Research and Innovation Program under Grant Agreement 963530. The authors acknowledge the financial support of the 3BCAR Institut Carnot for the acquisition of the Py-GC/MS equipment.

References

[1] L. Abdelouahed, S. Leveneur, L. Vernieres-Hassimi, L. Balland, and B. Taouk. Comparative investigation for the determination of kinetic parameters for biomass pyrolysis by thermogravimetric analysis. *Journal of Thermal Analysis and Calorimetry*, 129:1201–1213, 2017.

[2] A. V. Bridgwater. Review of fast pyrolysis of biomass and product upgrading. *Biomass and Bioenergy*, 38:68–94, 2012.

[3] T. Kan, V. Strezov, and T. J. Evans. Lignocellulosic biomass pyrolysis: A review of product properties and effects of pyrolysis parameters. *Renewable and Sustainable Energy Reviews*, 57:1126–1140, 2016.

[4] D. Mohan, C. U. Pittman Jr., and P. H. Steele. Pyrolysis of wood/biomass for bio-oil: A critical review. *Energy & Fuels*, 20(3):848–889, 2006.

[5] R. Muzyka, S. Sobek, M. Dudziak, M. Ouadi, and M. Sajdak. A comparative analysis of waste biomass pyrolysis in py-gc-ms and fixed-bed reactors. *Energies*, 16(8):3528, 2023.

[6] B. Shrestha, Y. Le Brech, T. Ghislain, S. Leclerc, V. Carré, F. Aubriet, S. Hoppe, P. Marchal, S. Pontvianne, N. Brosse, and Dufour A. A multitechnique characterization of lignin softening and pyrolysis. *ACS Sustainable Chemistry & Engineering*, 5(8):6940–6949, 2017.

[7] A. Meraj, S. P. Singh, M. Jawaid, M. M. Nasef, T. S. Alomar, and N. AlMasoud. A review on eco-friendly isolation of lignin by natural deep eutectic solvents from agricultural wastes. *Journal of Polymers and the Environment*, pages 1–34, 2023.

[8] J. Illingworth, P. T. Williams, and B. Rand. Characterisation of biochar porosity from pyrolysis of biomass flax fibre. *Journal of the Energy Institute*, 86(2):63–70, 2013.

[9] K. Malik, F. Ahmad, N. A. Yunus, E. Gunister, T. Nakato, E. Mouri, and S. Ali. A review of flax fiber reinforced thermoset polymer composites: Thermal-physical properties, improvements and application. *Journal of Natural Fibers*, 19(15):10412–10430, 2022.

[10] A. Melelli, F. Jamme, J. Beaugrand, and A. Bourmaud. Evolution of the ultrastructure and polysaccharide composition of flax fibres over time: When history meets science. *Carbohydrate Polymers*, 291:119584, 2022.

[11] B. Barthod-Malat, M. Hauguel, K. Behlouli, M. Grisel, and G. Savary.

Influence of the compression molding temperature on VOCs and odors produced from natural fiber composite materials. *Coatings*, 13(2):371, 2023.

[12] L. Ding, Y. Gong, Y. Wang, F. Wang, and G. Yu. Characterisation of the morphological changes and interactions in char, slag and ash during CO_2 gasification of rice straw and lignite. *Applied Energy*, 195:713–724, 2017.

[13] A. R. Reed and P. T. Williams. Thermal processing of biomass natural fibre wastes by pyrolysis. *International Journal of Energy Research*, 28(2):131–145, 2004.

[14] Q. Lu, B. Hu, Z. Zhang, Y. Wu, M. Cui, D. Liu, C. Dong, and Y. Yang. Mechanism of cellulose fast pyrolysis: The role of characteristic chain ends and dehydrated units. *Combustion and Flame*, 198:267–277, 2018.

[15] D. K. Shen and S. Gu. The mechanism for thermal decomposition of cellulose and its main products. *Bioresource Technology*, 100(24):6496–6504, 2009.

[16] D. Shen, W. Jin, J. Hu, R. Xiao, and K. Luo. An overview on fast pyrolysis of the main constituents in lignocellulosic biomass to valued-added chemicals: Structures, pathways and interactions. *Renewable and Sustainable Energy Reviews*, 51:761–774, 2015.

[17] D. K. Shen, S. Gu, and A. V. Bridgwater. Study on the pyrolytic behaviour of xylan-based hemicellulose using TG–FTIR and Py–GC–FTIR. *Journal of Analytical and Applied Pyrolysis*, 87(2):199–206, 2010.

[18] S.-F. Jiang, G.-P. Sheng, and H. Jiang. Advances in the characterization methods of biomass pyrolysis products. *ACS Sustainable Chemistry & Engineering*, 7(15):12639–12655, 2019.

[19] D. K. Shen, S. Gu, K. H. Luo, S. R. Wang, and M. X. Fang. The pyrolytic degradation of wood-derived lignin from pulping process. *Bioresource Technology*, 101(15):6136–6146, 2010.

[20] J. C. del Río, A. Gutiérrez, I. M. Rodríguez, D. Ibarra, and Á. T. Martínez. Composition of non-woody plant lignins and cinnamic acids by Py-GC/MS, Py/TMAH and FT–IR. *Journal of Analytical and Applied Pyrolysis*, 79(1-2):39–46, 2007.

[21] J. C. del Río, J. Rencoret, A. Gutiérrez, L. Nieto, J. Jiménez-Barbero, and Á. T. Martínez. Structural characterization of guaiacyl-rich lignins in flax (*linum usitatissimum*) fibers and shives. *Journal of Agricultural and Food Chemistry*, 59(20):11088–11099, 2011.

[22] W. Gieparda, S. Rojewski, and W. Różańska. Effectiveness of silanization and plasma treatment in the improvement of selected flax fibers' properties. *Materials*, 14(13):3564, 2021.

[23] A. Zolghadr, J. J. Biernacki, and R. J. Moore. Biomass fast pyrolysis using a novel microparticle microreactor approach: Effect of particles size, biomass type, and temperature. *Energy & Fuels*, 33(2):1146–1156, 2018.

[24] P. Ghorbannezhad, F. Kool, H. Rudi, and S. Ceylan. Sustainable production of value-added products from fast pyrolysis of palm shell residue in tandem micro-reactor and pilot plant. *Renewable Energy*, 145:663–670, 2020.

[25] C. He, F. Cao, Y. Wei, Z. Zhao, L. Cui, Y. Qin, S. V. Vassilev, and C. G. Vassileva. Morphological changes and ash fusibility of coal, rice straw and their mixture during co_2 gasification. *Fuel*, 292:120372, 2021.

[26] Y. Ma, Z. Ge, F. Li, Z. Zha, M. Zeng, and H. Zhang. Pyrolysis and co_2 gasification of biomass in high-temperature stage microscope: Morphological evolution and thermal behaviors. *Combustion and Flame*, 245:112387, 2022.

[27] J. Wei, Q. Guo, H. Chen, X. Chen, and G. Yu. Study on reactivity characteristics and synergy behaviours of rice straw and bituminous coal cogasification. *Bioresource Technology*, 220:509–515, 2016.

[28] Y. Ding, C. Wang, and S. Lu. Modeling the pyrolysis of wet wood using firefoam. *Energy Conversion and Management*, 98:500–506, 2015.

[29] J. Lachaud, J. B. Scoggins, T. E. Magin, M. G. Meyer, and N. N. Mansour. A generic local thermal equilibrium model for porous reactive materials submitted to high temperatures. *International Journal of Heat and Mass Transfer*, 108:1406–1417, 2017.

[30] S. Vikram, P. Rosha, and S. Kumar. Recent modeling approaches to biomass pyrolysis: A review. *Energy & Fuels*, 35(9):7406–7433, 2021.

[31] F. Torres-Herrador, V. Leroy, B. Helber, L. Contat-Rodrigo, J. Lachaud, and T. Magin. Multicomponent pyrolysis model for thermogravimetric analysis of phenolic ablators and lignocellulosic biomass. *AIAA Journal*, 58(9):4081–4089, 2020.

[32] H. Yang, R. Yan, H. Chen, D. H. Lee, and C. Zheng. Characteristics of hemicellulose, cellulose and lignin pyrolysis. *Fuel*, 86(12-13):1781–1788, 2007.

[33] M. Brebu and C. Vasile. Thermal degradation of lignin. *Cellulose Chemistry & Technology*, 44(9):353, 2010.

[34] J. Chaishome, K. A. Brown, R. Brooks, and M. J. Clifford. Thermal degradation of flax fibres as potential reinforcement in thermoplastic composites. *Advanced Materials Research*, 894:32–36, 2014.

[35] G. Dorez, B. Otazaghine, A. Taguet, L. Ferry, and J. M. Lopez-Cuesta. Use of py-gc/ms and pcfc to characterize the

surface modification of flax fibres. *Journal of Analytical and Applied Pyrolysis*, 105:122–130, 2014.

[36] H. El Bari, C. K. Fanezoune, B. Dorneanu, H. Arellano-Garcia, T. Majozi, Y. Elhenawy, O. Bayssi, A. Hirt, J. Peixinho, A. Dhahak, M. A. Gadalla, N. H. Khashaba, and F. H Ashour. Catalytic fast pyrolysis of lignocellulosic biomass: Recent advances and comprehensive overview. *Journal of Analytical and Applied Pyrolysis*, page 106390, 2024.

[37] J. Leboucher, P. Bazin, D. Goux, H. El Siblani, A. Travert, A. Barbulée, J. Bréard, and B. Duchemin. High-yield cellulose hydrolysis by hcl vapor: co-crystallization, deuterium accessibility and high-temperature thermal stability. *Cellulose*, 27:3085–3105, 2020.

[38] C. A. Schneider, W. S. Rasband, and K. W. Eliceiri. NIH Image to ImageJ: 25 years of image analysis. *Nature Methods*, 9(7):671–675, 2012.

[39] G. Lv and S. Wu. Analytical pyrolysis studies of corn stalk and its three main components by TG–MS and Py-GC/MS. *Journal of Analytical and Applied Pyrolysis*, 97:11–18, 2012.

[40] B. Babinszki, E. Jakab, V. Terjék, Z. Sebestyén, G. Várhegyi, Z. May, A. Mahakhant, L. Attanatho, A. Suemanotham, Y. Thanmongkhon, and Z. Czégény. Thermal decomposition of biomass wastes derived from palm oil production. *Journal of Analytical and Applied Pyrolysis*, 155:105069, 2021.

[41] W.-H. Chen, C.-W. Wang, G. Kumar, P. Rousset, and T.-H. Hsieh. Effect of torrefaction pretreatment on the pyrolysis of rubber wood sawdust analyzed by Py-GC/MS. *Bioresource Technology*, 259:469–473, 2018.

[42] I. Itabaiana Junior, M. A. Do Nascimento, R. O. M. A. de Souza, A. Dufour, and R. Wojcieszak. Levoglucosan: A promising platform molecule? *Green Chemistry*, 22(18):5859–5880, 2020.

[43] M. R. Rover, A. Aui, M. M. Wright, R. G. Smith, and R. C. Brown. Production and purification of crystallized levoglucosan from pyrolysis of lignocellulosic biomass. *Green Chemistry*, 21(21):5980–5989, 2019.

[44] S. Guo, H. Liang, D. Che, H. Liu, and B. Sun. Quantitative study of the pyrolysis of levoglucosan to generate small molecular gases. *RSC Advances*, 9(33):18791–18802, 2019.

[45] B. He, Y. Yu, X. Gong, S. Liu, H. Tian, and E. Leng. Mechanism of acid-catalyzed pyrolysis of levoglucosan: Formation of anhydro-disaccharides. *Fuel*, 345:128242, 2023.

[46] X. Zhang, W. Yang, and C. Dong. Levoglucosan formation mechanisms during cellulose pyrolysis. *Journal of Analytical and Applied Pyrolysis*, 104:19–27, 2013.

[47] Y. Huang, D. T. Sekyere, J. Zhang, and Y. Tian. Fast pyrolysis behaviors of biomass with high contents of ash and nitrogen using TG–FTIR and Py-GC/MS. *Journal of Analytical and Applied Pyrolysis*, 170:105922, 2023.

[48] D. K. Shen and S. Gu. The mechanism for thermal decomposition of cellulose and its main products. *Bioresource Technology*, 100(24):6496–6504, 2009.

[49] D. O. Usino, Supryanto, P. Ylitervo, A. Pettersson, and T. Richards. Influence of temperature and time on initial pyrolysis of cellulose and xylan. *Journal of Analytical and Applied Pyrolysis*, 147:104782, 2020.

[50] Supryanto, D. O. Usino, P. Ylitervo, J. Dou, M. H. Sipponen, and T. Richards. Identifying the primary reactions and products of fast pyrolysis of alkali lignin. *Journal of Analytical and Applied Pyrolysis*, 151:104917, 2020.

[51] X. Xin, S. Pang, F. de Miguel Mercader, and K. M. Torr. The effect of biomass pretreatment on catalytic pyrolysis products of pine wood by Py-GC/MS and principal component analysis. *Journal of Analytical and Applied Pyrolysis*, 138:145–153, 2019.

[52] L. Chen, Y. Liao, Z. Guo, Y. Cao, and X. Ma. Products distribution and generation pathway of cellulose pyrolysis. *Journal of Cleaner Production*, 232:1309–1320, 2019.

[53] C. Mohabeer, L. Abdelouahed, S. Marcotte, and B. Taouk. Comparative analysis of pyrolytic liquid products of beech wood, flax shives and woody biomass components. *Journal of Analytical and Applied Pyrolysis*, 127:269–277, 2017.

Table 1: The main chemical compounds of flax fibers by Py-GC/MS

Peak number	Retention time min	Compound	Chemical formula	Chemical family
1	3.97	2-Butenal, 2-methyl	$C_4H_4O_2$	Aldehydes
2	4.27	1,2:5,6-Dianhydrogalactitol	$C_6H_{10}O_4$	Anhydrosugars
3	4.75	3(2H)-Furanone	$C_4H_4O_2$	Furans
4	5.03	3-Furaldehyde	$C_5H_4O_2$	Furans
5	5.2	3-Furanmethanol	$C_5H_6O_2$	Furans
6	5.45	Furfural	$C_5H_4O_2$	Furans
7	5.89	2-Furanmethanol	$C_5H_6O_2$	Furans
8	6.54	4-Cyclopentene-1,3-dione	$C_5H_4O_2$	Ketones
9	7.22	2(5H)-Furanone	$C_4H_4O_2$	Furans
10	7.4	1,2-Cyclopentanedione	$C_5H_6O_2$	Ketones
11	8.44	5-Methylfurfural	$C_6H_6O_2$	Furans
12	9.14	2H-Pyran-2,6(3H)-dione	$C_5H_4O_3$	Ketones
13	9.26	2,2-Diethyl-3-methyl-oxazolidine	C_8H_17NO	Others
14	9.6	3-Methyl-1,2-cyclopentanedione	$C_6H_8O_2$	Ketones
15	10	2-Cyclopenten-1-one, 2-hydroxy-3-methyl-	$C_6H_8O_2$	Ketones
16	10.35	3(2H)-furanone, dihydroxy-5-isopropyl	$C_7H_{12}O_2$	Furans
17	10.59	5-(Hydroxymethyl)dihydrofuran-2(3H)-one	$C_5H_8O_3$	Furans
18	11.4	3-Furancarboxylic acid, methyl ester	$C_6H_6O_3$	Furans
19	11.66	3-Butene-1,2-diol	$C_4H_8O_2$	Alcohols
20	12.1	Maltol	$C_6H_6O_3$	Ketones
21	12.37	4,5-Dihydro-3-furoic acid	$C_5H_6O_3$	Furans
22	13.3	2(3H)-Furanone, dihydro-4-hydroxy-	$C_4H_6O_3$	Furans
23	13.95	1,4:3,6-Dianhydro-α-D-glucopyranose	$C_6H_8O_4$	Anhydrosugars
24	14.19	Catechol	$C_6H_6O_2$	Phenols
25	14.67	Benzaldehyde, 3-methyl-	C_8H_8O	Aldehydes
26	14.92	5-Hydroxymethylfurfural	$C_6H_6O_3$	Furans
27	15.38	1-Phenoxypropan-2-ol	$C_9H_{12}O_2$	Phenols
28	16.32	4-Methylcatechol	$C_7H_8O_2$	Phenols
29	16.57	5-Hydroxy-2-(hydroxymethyl)-2,3-dihydro-4H-pyran-4-one	$C_6H_8O_4$	Ketones
30	16.91	4-Vinylguaiacol	$C_9H_{10}O_2$	Phenols
31	17.59	Syringol	$C_8H_{10}O_3$	Phenols
32	17.83	1,6-Anhydro-β-d-talopyranose	$C_6H_{10}O_5$	Anhydrosugars
33	18.41	Vanillin	$C_8H_8O_3$	Phenols
34	19.17	trans-Isoeugenol	$C_{10}H_{12}O_2$	Phenols
35	19.58	Levoglucosan	$C_6H_{10}O_5$	Anhydrosugars
36	19.7	6-Methoxy-3-methylbenzofuran	$C_{10}H_{10}O_2$	Furans
37	21.36	1,6-Anhydro-α-d-galactofuranose	$C_6H_{10}O_5$	Anhydrosugars
38	22.49	Coniferyl aldehyde	$C_{10}H_{10}O_3$	Phenols
39	22.49	α,β-Dihydroferulic acid, ethyl ester	$C_{12}H_{16}O_4$	Esters
40	24.46	Palmitic acid	$C_{16}H_{32}O_2$	Acids